PHYSICAL REVIEW B

CONDENSED MATTER

THIRD SERIES, VOLUME 33, NUMBER 1 1 JANUARY 1986

Magnetic structure and dynamics in the α and β phases of solid oxygen

Peter W. Stephens
Department of Physics, State University of New York, Stony Brook, New York 11794

C. F. Majkrzak
Department of Physics, Brookhaven National Laboratory, Upton, New York 11973
(Received 24 June 1985)

We describe a comprehensive neutron scattering study of α- and β-O_2. In α-O_2, an inelastic feature at 10 meV is identified with the $b^*/2$ zone boundary, enabling the first measurement of the intrasublattice exchange in this system. We find the intrasublattice exchange constant to be -1.2 ± 0.1 meV. Taken in conjunction with the intersublattice exchange, -2.4 meV determined from magnetic susceptibility, we find that the system is very close to a magnetic instability. The α-phase staggered magnetization drops with increasing temperature, extrapolating to a purely magnetic transition at 31 K, which is 7 K above the α-β transition. This is only 40% of the mean-field ordering temperature, implying that the magnetic couplings are predominantly two-dimensional (2D). β-O_2 has 2D short-range magnetic correlations. These results are discussed in light of a model of magnetoelastic coupling in a frustrated triangular antiferromagnet.

I. INTRODUCTION

The magnetism of solid oxygen has generated much confusion. α-O_2 is one of the only localized-spin systems in which the exchange interaction results from the direct overlap of magnetic orbitals. Nevertheless, no complete description of the magnetic behavior has yet been accepted. One can identify two reasons for this difficulty: the lack of sufficiently large single crystals required for many measurements, and the interaction of magnetic and lattice degrees of freedom.

In this paper we describe a series of elastic and inelastic neutron scattering experiments on powders of α- and β-O_2. The techniques used enable us to separate lattice and magnetic excitations, and to study the elementary excitations as a function of momentum and energy. A consistent picture of the magnetic structure of both phases, as well as the mechanism for the α-β transition, emerges from our analysis.

Magnetically, the low-temperature phases of O_2 can be modeled with antiferromagnetic interactions on a two-dimensional (2D) triangular lattice. The fact that no arrangement of classical spins satisfies the magnetic interactions suppresses the transition temperature, so that β-O_2 has only short-range magnetic order. α-O_2 circumvents the magnetic frustration by means of a lattice distortion, so that a two-sublattice magnetic structure is favored. Each spin has four nearest neighbors on the opposite magnetic sublattice, and two next-nearest neighbors on the same sublattice. It is quite plausible that the competition between the relief of magnetic frustration and the elastic strain energy results in a ratio of next-nearest to nearest-neighbor magnetic interactions which is less than unity, but not negligible.

We review the current status of knowledge of the magnetic interactions in α-O_2 in Sec. II, and present our neutron measurements on α- and β-O_2 in Sec. III. Section IV discusses the implications of this work, particularly in reference to the α-β transition. This work has been summarized in a preliminary communication.[1]

II. REVIEW OF MAGNETIC INTERACTIONS IN α-O_2

The choice of magnetic interaction parameters in α-O_2 has been rather controversial, with different experiments yielding apparently vastly different results. In a comprehensive survey, DeFotis was unable to bring all of the work into accord.[2] In this section we review some of the previous work, with a particular emphasis on optical properties and susceptibility.

The inset to Fig. 1 shows the lattice and magnetic structure of α-O_2. The structure is derived from a rhombodedral lattice of stacked triangular sheets by a small distortion within the basal plane. Magnetically, α-O_2 is a two-sublattice antiferromagnet (AF), with spins that are oriented in the plane, directed along lines parallel to the b

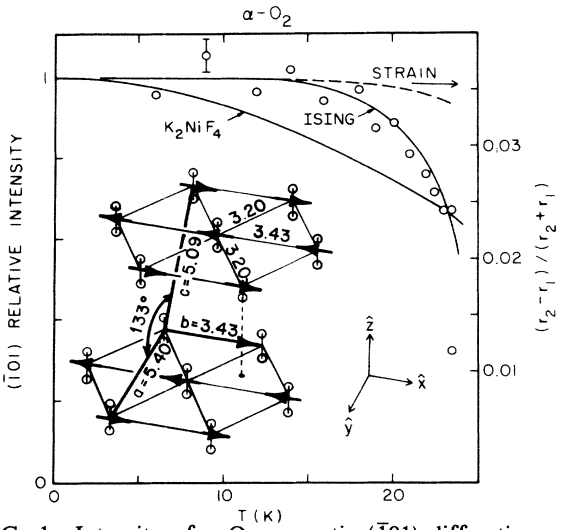

FIG. 1. Intensity of α-O_2 magnetic ($\bar{1}01$) diffraction peak versus temperature. Smooth curves show the sublattice magnetization for K_2NiF_4 (Ref. 3) and the Ising model (Ref. 4). Dashed line shows the in-plane lattice strain determined from Ref. 5. Inset shows the lattice and magnetic structure of α-O_2 (Refs. 5–7). The conventional unit cell, indicated by monoclinic translation vectors, contains two molecules, and is also the magnetic cell.

axis.[7] Each spin is therefore surrounded by four nearest neighbors on the opposite magnetic sublattice, and two next-nearest neighbors on the same sublattice, all within the same *ab* plane. The nearest neighbors on the adjacent planes are also on the opposite sublattice.

The magnetic electrons in the O_2 molecule come from one unpaired $2p$ atomic orbital on each atom. Hund's rules imply that these combine to form a ground state with orbital angular momentum $L=0$ and spin $S=1$. Various interactions within the free molecule and between molecules in the solid act to split the single-molecule ground state.

We describe the magnetic system with the spin Hamiltonian,

$$H=-2\sum_{\langle ij\rangle}J_{ij}\mathbf{S}_i\cdot\mathbf{S}_j+\sum_i(-DS_{xi}^2-D'S_{yi}^2+D'S_{zi}^2)\ . \quad (1)$$

Here the x and z axes are in the average spin (b-axis) and molecular (c^* axis) directions, respectively. The first sum runs over pairs $\langle ij\rangle$ of sites with a non-negligible exchange interaction. In the present case, J_{ij} takes the value J_{NN} for four nearest neighbors in the *ab* plane, which are on the opposite magnetic sublattice, J_{NNN} for the intrasublattice interaction with two next-nearest neighbors in the plane, and $J_\perp$ to four opposite sublattice neighbors on adjacent *ab* planes. Because the exchange interaction depends on the overlap of orbitals, one expects that J drops rapidly with increasing intermolecular separation. For this reason, we neglect further neighbors. If $D=D'>0$, the model has easy-plane magnetization-(XY) anisotropy; if $D>0$ and $D'=0$, the anisotropy is Ising-like.

In general, the most straightforward probe of magnetic properties is the magnetic susceptibility. In the limit of low temperature, the mean-field susceptibility of the Néel state of a two-sublattice AF, for applied field perpendicular to the spin easy-magnetization axis, is given by

$$\chi_\perp^{MF}=\frac{N_A g^2\mu_B^2}{4|J|}\ . \quad (2)$$

Here J is the sum of all intersublattice exchange constants. In the present case, $J=4J_{NN}+4J_\perp$. Corrections to the Néel state enter through a multiplicative factor,

$$\chi_\perp=[1-\Delta S/S-i(\alpha)]\chi_\perp^{MF}\ . \quad (3)$$

The two corrections are due to spin-wave corrections to the Néel state; the first is due to the change in magnetization, the second to corrections to the ground-state energy.[8,9] Both terms depend weakly on the anisotropy via the parameter α, defined as $(DD')^{1/2}/(z|J|)$, where z is the number of neighbors. Based on the exchange and anisotropy parameters discussed below, α is approximately 0.01, a sufficiently small value that the $\alpha=0$ value of these corrections may be taken.

In view of the uncertainty of the dimensionality of the magnetic coupling, we consider both 2D and three-dimensional (3D) values of these corrections. For the Heisenberg AF on a square lattice, Lines and Colpa *et al.* give $\Delta S=0.197$ and $i(0)=0.08$.[10] In three dimensions, both corrections are significantly smaller: $\Delta S=0.078$ and $i(0)=0.04$. We therefore see that the spin-wave correction lowers the susceptibility of a 2D Heisenberg magnet by 28%, and that of a 3D magnet by 12%.

Experimentally, DeFotis has determined $\chi_\perp=(2.4\pm0.03)\times10^{-3}$ cm^3/mole.[2] Meier, Schinkel and deVisser[11] are in agreement, with a published value of 2.46×10^{-3}. The mean-field analysis then leads to intersublattice exchange $J_{NN}+J_\perp=-3.4$ meV$=-39$ K. Corrections for spin deviation decrease this number as much as 28%, depending on the dimensionality.

DeFotis[2] and Meier *et al.*[11] have presented this value for J_{NN}, without the spin-wave corrections. Meier *et al.* have also argued that the dependence of the susceptibility on temperature through the α and β phases can be explained by assuming a power law variation of exchange interaction on intermolecular separation, modeling the β phase as an ordered two-sublattice AF. They have further extended this analysis to the pressure dependence of the susceptibility of α and γ phases.[11] This leads to an estimate of the intrasublattice exchange of $J_{NNN}=-0.9$ meV.[11]

We next take up a discussion of the magnetic dynamics in α-O_2. Lindgard *et al.*[12] give the magnon spectrum for the Hamiltonian of Eq. (1) with $S=1$,

$$E_a^2(\mathbf{q})=(2J_0-2J_q-2J_0'+D)^2-[2J_q'+(-1^a)D']^2\ , \quad (4)$$

where $J_\mathbf{q}=\sum_i J_i e^{i\mathbf{q}\cdot\mathbf{r}_i}$ with the sum running over neighbors on the same sublattice, and J_q' is similarly defined for opposite sublattice neighbors. $a=\{0,1\}$ is the branch index. To lowest order, the ground-state-energy correction discussed above also increases all of the spin-wave energies by a factor $1+i(\alpha)$.[8] We note several differences with other published magnon dispersion relations. Marshall and Lovesey treat the case of Ising-like anisotro-

TABLE I. Magnon energies at $\mathbf{q}=0$ and zone boundaries, calculated from Eq. (4). The lowest-order correction for spin deviation multiplies these energies by $1+i(\alpha)$ (Ref. 8).

q	$E(\mathbf{q})$
(0,0,0)	$[(-16J_{NN}-16J_{\perp})(D\pm D')]^{1/2}$
$(\frac{1}{2},0,0),(\frac{1}{2},0,-\frac{1}{2})$	$-8J_{NN}-8J_{\perp}+D$
$(0,\frac{1}{2},0)$	$-8J_{NN}-8J_{\perp}+8J_{NNN}+D$
$(0,0,\frac{1}{2})$	$[(-8J_{NN}-8J_{\perp}+D)^2-(-8J_{NN}+8J\pm D')^2]^{1/2}$

py of the form $\pm\mu S_x H_A$, with anisotropy field H_A.[13] Their results are the same as Eq. (4) with $D'=0$, except for a factor of 2 in the anisotropy. This is evidently the result of carrying out one fewer term in the $1/S$ expansion of the Holstein-Primakof transformation. Several other authors have ignored or incorrectly treated intrasublattice couplings and give expressions which are approximately the same as Eq. (4).[14–17] The difference appear to lie in the order in which approximations are made in deriving the dispersion relation.

In the following we will be concerned with magnon densities of states, and in particular with the peaks of the density of states at zone-boundary (ZB) energies. The ZB energies are listed in Table I.

Wachtel and Wheeler identified two antiferromagnetic resonance (AFMR) modes at 6.4 and 27.5 cm^{-1} in infrared absorption.[14] Their magnetic nature is demonstrated by the fact that the energies depend upon applied magnetic field. Meier *et al.* have extended these measurements to higher fields, and have shown that single-molecule anisotropies derived from the free-molecule value [$D+D'=0.5$ meV (Ref. 18)] and the calculated magnetic dipole energy are unable to match the observed antiferromagnetic resonance frequencies.[17] They suggested magnon-phonon hybridization as a possible explanation for the observed frequency shifts.

The optical-absorption spectrum of α-O_2 is dominated by double-molecule transitions with a rather complicated sideband structure.[19] The absorption lines are generally blue-shifted by some 75 cm^{-1} relative to the free-molecule energies. Evidently, the absorption of light is accompanied by the creation of excitons, magnons, etc. Wachtel and Wheeler interpreted the 75-cm^{-1} shift in the double-molecule transitions as twice the energy of the excited state of a single molecule in the environment of the crystal.[14] They assumed all intersublattice exchanges were equal. In that case, there is one zone-boundary energy, which is essentially equal to the single-molecule excitation energy, leading to exchange energy $J_{NN}=J_{\perp}=-0.25$ meV.

Bhandari and Falicov have presented a more detailed model of the intermolecular interactions which is compatible with all of the details of the optical-absorption spectra.[20] They regard the derived parameters as being only a rough estimate, but they are in close agreement with the present work.

The relative strength of intra- and interplanar exchange interactions has been widely discussed, with no real consensus. The nearest-neighbor spins on adjacent planes have oppositely directed spins,[6] implying that $J_{\perp}<0$. Burakhovich *et al.* argued that $r_{NN}<r_{\perp}$ implies $|J_{NN}| \gg |J_{\perp}|$. They proposed a model in which 37.5 cm^{-1} was the zone boundary perpendicular to the planes and 75 cm^{-1} was the in-plane zone boundary.[15] Little justification was given for that particular assignment of energies. Slyusarev *et al.* sought another means to determine the relative inter- and intraplanar exchanges.[16] They fixed the easy-plane single-molecule anisotropy $D+D'$ at the free-molecule value of 4 cm^{-1}, and set an average zone-boundary energy to 37.5 cm^{-1}. This resulted in $J_{\perp}/J_{NN}=0.01$, and $J_{NN}=22$ meV. The result is meaningless, based as it is on the assumption of a single zone-boundary energy in an anisotropic system.

Clearly, the prime difficulty with these accounts is the fact that it is not clear what ZB magnon energy dominates the optical absorption. Except for Bhandari and Falicov, all of these interpretations have ignored the significance of the intrasublattice interaction, and the exchange constants derived are incompatible with the magnetic susceptibility.

Several groups have tried to determine J_{NN} and $J_{\perp}$ from less direct methods, such as magnon heat capacity,[2,5,15] parallel susceptibility,[2] or AFMR frequencies with assumed anisotropy.[2,16] These measurements disagree with the exchange derived from $\chi_{\perp}$, leading some authors to claim that there is a large uncertainty in the experimental determinations of interaction parameters.[2,21,22] This criticism is unjustified, inasmuch as the analysis of indirect experiments is based upon generally weak assumptions, such as the accuracy with which phonon heat capacity may be subtracted, the applicability of magnon theory at high temperature, and the neglect of crystal field energies. We emphasize that the susceptibility measurements are in good agreement, with the largest uncertainty in the determination of $J_{NN}+J_{\perp}$ arising from the spin deviation correction.

More recently, the intrasublattice exchange J_{NNN} has attracted some attention. Krupskii *et al.* inferred that $J_{NNN}<0$ from precise measurements of the lattice constants.[5] They noted that the thermal expansion coefficient along the monoclinic b axis was negative near the α-β transition temperature. Because the magnetization decreases with increasing temperature, this implies a magnetic repulsion between molecules on the same sublattice. They were not able to quantify this relation, partly because they had no direct measurement of the staggered

magnetization.

The first measurement of J_{NNN} was given in a previous communication by the present authors.[1] Inelastic polarized neutron scattering shows a distinct maximum at 10 meV (81 cm^{-1}). The basic strength of the neutron scattering technique is the fact that the cross section can be modeled quantitatively. We have interpreted this as a peak in the magnon density of states at a zone boundary; model calculations show that the $b^*/2$ energy strongly dominates the density of states. This implies that $J_{NNN}-J_{NN}-J_\perp \cong -1.2$ meV. Temporarily assuming that the couplings are 2D ($J_\perp=0$), the susceptibility leads to a spin-wave corrected $J_{NN}\cong -2.4$ meV, so that $J_{NNN}\cong -1.2$ meV. In Sec. III we present the model calculations and discuss this interpretation in full.

On the theoretical front, van Hemert *et al.* performed an *ab initio* calculation of the magnetic interaction between O_2 molecules.[21] They found $J_{NN}=-1.08$ meV, and suggested that lattice motions might increase the effective exchange toward the experimental value. For molecules oriented parallel as in α-O_2, their exchange may be represented as $J(R)\propto \exp(-R/0.27\ \text{Å})$, which implies a value of $J_{NNN}/J_{NN}=0.42$. Finally, their calculated $J_\perp$ was $+0.05$ meV, but they argued that an appropriate average over lattice motions could change the sign of this number. The coupling between magnetic and lattice degrees of freedom has been considered in greater detail by Jansen and van der Avoird, who show that the lattice motions actually *decrease* the effective exchange slightly to -1.0 meV.[22]

III. EXPERIMENTAL RESULTS

The samples of solid oxygen were prepared by condensing oxygen gas of 99.98% nominal purity in a cylindrical cell, 1.0 cm diameter by 2.5 cm long. This was cooled through the γ phase into the β and α phases in approximately one hour. The experiments were performed on the H-4 and H-8 spectrometers at the High Flux Beam Reactor at Brookhaven National Laboratory.

We performed several checks for preferred orientation in the sample. ω scans about the sample axis showed a variation of 10% (standard deviation) in the β-O_2 ($\bar{1}01$) and (003) (hexagonal indices) Bragg peaks. The ratio of these two intensities was 2.1, compared with an expected ratio of 4.9 (product of multiplicity, structure factor squared, Lorentz factor, and Debye-Waller factor[5–7]). We therefore conclude that there is little preferential orientation within the plane, but that the hexagonal c axis tends to be oriented along the sample axis. Deviations from a random powder of this magnitude do not have a qualitative effect on the interpretation of the present experiment.

A. α phase, diffraction

Figure 1 shows the temperature variation of the magnetic ($\bar{1}01$) diffraction peak, measured with pyrolytic graphite (002) monochromator and analyzer, 20′-40′-40′-40′ collimation, and a pyrolytic graphite filter. The incident neutron beam was masked to 6 mm height, in order to minimize possible thermal gradients in the sample. The intensity of this peak is proportional to the square of the sublattice magnetization. The data were taken on warming. At 23.5 K, we observed a slow conversion from α to β phase. Note, however, that no β-O_2 diffraction peaks were seen in any scan below this temperature. The square of the staggered magnetization has fallen to roughly 65% of its saturated value at the first-order α-β transition. The magnetization curve was the same on cooling, with hysteresis of approximately 2 K at the transition. It is of interest to compare this magnetization curve with other systems. The smooth curves in Fig. 1 show the diffraction peak intensity in K_2NiF_4, a planar Heisenberg AF,[3] and the square of the magnetization for the 2D Ising model on a square lattice.[4] While the data for α-O_2 do not get sufficiently close to a purely magnetic transition to make any judgment of critical behavior, the shape of the magnetization curve is certainly more similar to that of the Ising system then the continuous-symmetry Heisenberg magnet. Evidently, if the α-O_2 lattice were held rigid, the magnetic order would disappear at a critical temperature in the range 25–32 K.

Also shown is the in-plane distortion determined by Krupskii *et al.*[5] It is evident that the loss of magnetic order due to thermal fluctuations is stronger than the relaxation of the strain. We will return to a discussion of the coupled magnetic and lattice degrees of freedom at the α-β transition in Sec. IV.

B. α phase, inelastic

In the ideal case of a single-crystal sample, neutron spectroscopy can be used to map out the dispersion curves of phonons or magnons. Hence, the main obstacle to the determination of magnetic exchange parameters is the lack of single crystals of α-O_2. Nevertheless, it is possible to obtain significant information about the magnetic dynamics from inelastic scattering measurements on powders. For a powder sample, one may crudely think of the inelastically scattered neutron intensity as a measure of the density of states at specified energy and magnitude of the scattering wave vector $|\mathbf{Q}|$. For a detailed analysis, one must take into account the neutron scattering cross section, which depends on $\mathbf{Q}$. In general, a neutron interacts with both the nuclei and the magnetic moments of a target. In order to restrict our attention to the magnetic subsystem, we have applied polarized scattering techniques to this system.

The polarized neutron measurements were made with Heusler alloy monochromator and analyzer, with 0.2-T guide fields arranged so that the neutron spin parallel to the scattering vector was resolved. In this configuration, magnetic interactions flip the neutron spin, whereas nuclear scattering does not.[23] These measurements were made with a constant final neutron energy of 31.4 meV, 40′-40′-open-40′ collimation, and no filter. The second-order reflections from the monochromator and analyzer are essentially unpolarized. Any feature in the inelastic spectra due to second-order contamination would therefore appear equally in both flipper-on and flipper-off channels. The flipping ratio was $R=10$. We corrected for the finite flipping ratio by subtracting a fraction $1/R$ of the signal with the flipper off from that with the

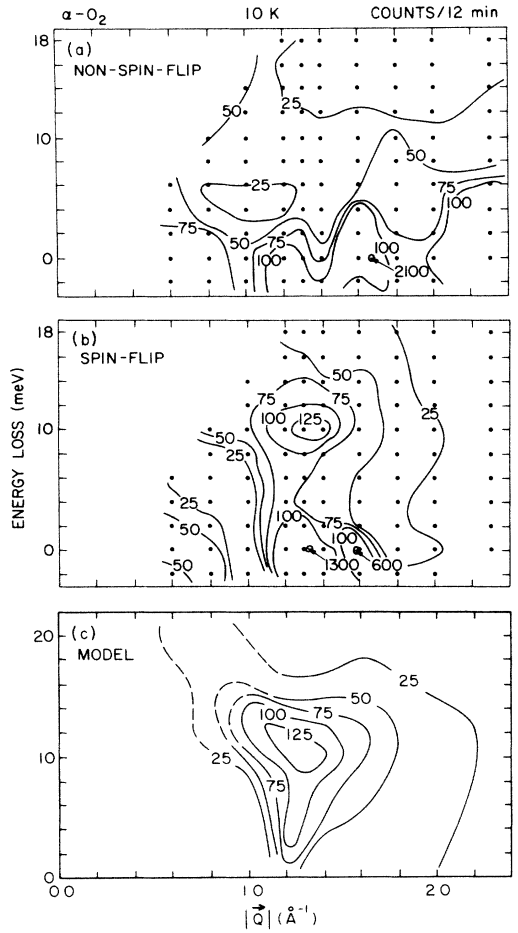

FIG. 2. Panels (a) and (b) show the non-spin-flip and spin-flip inelastically scattered neutron intensity from powders of α-O_2. Panel (c) shows the result of the model calculation discussed in the text for 2D magnetic coupling parameters, $J_{NN}=-2.44$ meV, $J_{NNN}=-1.22$ meV, $J_\perp=0$, $D+D'=0.25$, $D-D'=0.014$.

flipper on, to obtain the spin-flip cross section, and likewise for the non-spin-flip cross section.

The resulting contour map of intensity as a function of the magnitude of neutron momentum difference and energy loss is shown in Fig. 2. The magnetic $(\bar{1}01)$ and (100) Bragg peaks are visible in the spin-flip intensity at 1.32 and 1.58 Å^{-1}; the nuclear (001) Bragg peak at 1.68 Å^{-1} is in the non-spin-flip channel. Scans at selected wave vectors, extended to higher energy, did not reveal any further excitations.

The principal inelastic feature seen in the data of Fig. 2 is the peak at 1.3 Å^{-1}, 10 meV. This feature is nearly resolution limited in energy. The analysis of this data is based on the identification of this 10-meV feature with a peak in the magnon density of states. An alternative interpretation, that of magnetovibrational scattering, is dismissed in the Appendix.

The total intersublattice exchange, $J_{NN}+J_\perp$, is determined from the susceptibility. Using the ZB energies from Table I, we see that this implies that the $(\frac{1}{2},0,0)$ and $(-\frac{1}{2},0,\frac{1}{2})$ ZB energies are on the order of 20 meV, independent of the relative magnitudes of J_{NN} and $J_\perp$. If this were the only singularity in the density of states, it would appear to contradict the description of the 10-meV feature as a ZB magnon. However, Table I shows that the $(0,\frac{1}{2},0)$ ZB can have a lower energy, depending on the value of J_{NNN}.

We proceed by considering the magnon density of states for the dispersion relation given by Eq. (4). Figure 3 shows the magnon dispersion curves along several directions for three different choices of exchange parameters. In all three cases, the total intrasublattice exchange was chosen to agree with the spin-wave-corrected magnetic susceptibility, as described in Sec. II. We calculated the magnon density of states by sampling points at random within the first Brillouin zone. The strongest contribution to the magnon density of states comes from the van Hove singularity at the $(0\ \frac{1}{2}\ 0)$ ZB. This observation may be explained by noting that this point is a saddle point in the dispersion relations, so that the constant-energy surface at this energy covers a large region of the interior of the zone. Figure 3 shows that this is the case regardless of whether 2D or 3D magnetic exchange couplings are chosen.

Figure 3(a) points up an interesting effect: If $-J_{NNN}>-(J_{NN}+J_\perp)/2$, the calculated spin-wave energy becomes imaginary for a region along the (010) direction. This is a manifestation of the fact that the Néel state is unstable for sufficiently strong antiferromagnetic intrasublattice exchange.[24]

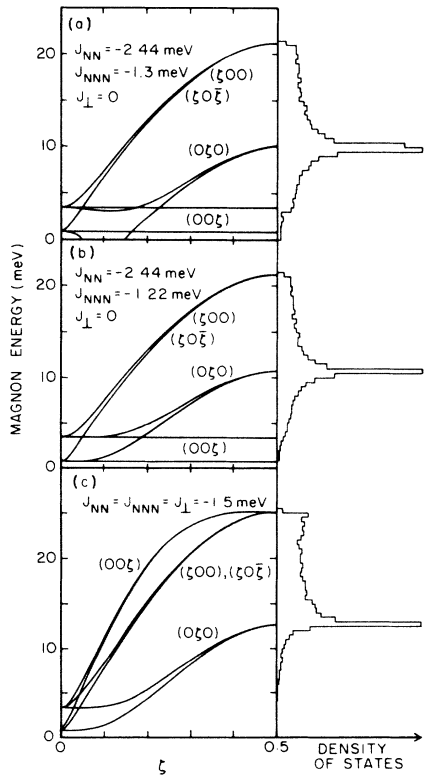

FIG. 3. Magnon dispersion curves and density of states for three sets of magnetic interaction parameters, constrained to agree with the experimentally determined AFMR energies and the magnetic susceptibility of α-O_2.

In order to confirm the assignment of the 10-meV ridge in the inelastic neutron scattering measurements as the peak in the density of states at the $(0\ \frac{1}{2}\ 0)$ ZB energy, we have calculated the distribution of inelastically scattered neutrons from a powder. Such a model calculation is necessary because the neutron scattering measurements are performed at specified wave vectors rather than averaged over the entire zone, and the cross section has a rather complicated dependence on wave vector.

Marshall and Lovesey[13] give the dynamical structure factor for the creation of one magnon in an AF as

$$S(\mathbf{Q},\omega)=(1+\hat{\mathbf{Q}}_x^2)[u_\mathbf{q}+(-1^m)v_\mathbf{q}]^2 \times\delta(E_a(\mathbf{q})-\hbar\omega)\delta(\mathbf{Q}-\mathbf{q}-\tau)\ . \quad (5)$$

Here, $\hbar\omega$ is the neutron energy loss, $\hbar^2(k_i^2-k_f^2)/2M$, $\hat{\mathbf{Q}}_x$ is the component of the unit vector along $\mathbf{Q}$ in the spin ($\hat{\mathbf{x}}$) direction, $\mathbf{q}$ is a vector in the first Brillouin zone, and τ is an element of the (magnetic) reciprocal lattice. $m=0$ if τ is a nuclear peak (Miller indices $h+k$ even), 1 if τ is a magnetic peak ($h+k$ odd). The factor $[u_\mathbf{q}+(-1^m)v_\mathbf{q}]^2$ depends on the Holstein-Primakof transformation coefficients. We take[25]

$$[u_\mathbf{q}+(-1^m)v_\mathbf{q}]^2 =2S\frac{2J_0-2J_0'-2J_\mathbf{q}+D-(-1^m)[2J_\mathbf{q}'+(-1^a)D']}{E_a(\mathbf{q})}\ .$$

This contains the strongest dependence of the magnon cross section on energy, approximately $[E(\mathbf{q})]^{-1}$ in a zone with an allowed antiferromagnetic diffraction Bragg peak.

The neutron scattering cross section $\sigma(\mathbf{Q},\omega)$ is proportional to[26]

$$\exp(-2W)[n(\hbar\omega)+1]F^2(\mathbf{Q})S(\mathbf{Q},\omega)\ ,$$

where $\exp(-2W)$ is the Debye-Waller factor, $n(E)$ is the Bose factor $[\exp(-E/kT)-1]^{-1}$, and $F(\mathbf{Q})$ is the magnetic form factor.[27]

In the experimental data of Fig. 2, the neutron scattering cross section in a powder sample was measured as a function of the energy loss $\hbar\omega$ and magnitude of scattered wave vector $\mathbf{Q}$. These data are compared with the orientationally-averaged cross section,

$$\sigma_p(Q,\omega)=\int d\Omega_\mathbf{Q}\,\sigma(\mathbf{Q},\omega)\ .$$

We calculated this integral by sampling $\Omega_\mathbf{Q}$ at random, calculating $E_a(\mathbf{Q})$, and accumulating $\sigma(Q,\omega)$ into bins 1 meV wide.

Finally, the powder-averaged structure factor must be convoluted with the spectrometer resolution function. The resolution ellipse, obtained by integrating the Cooper-Nathans[28] resolution function over the transverse component of $\mathbf{Q}$, is nearly aligned with the momentum and energy axes at the point (1.5 Å^{-1}, 10 meV), where it has half width at half maximum (HWHM) of 0.05 Å^{-1} in Q and 2.5 meV in energy. Away from this point, it is tipped, so that the experiment integrates over a somewhat larger range of wave vectors. Nevertheless, its projection remains sharper in Q than the calculated variation of σ_p. The resolution correction therefore consists only of a convolution of $\sigma_p(Q,\omega)$ with a Gaussian of 2.5 meV HWHM in $\hbar\omega$.

The resulting contours for the case of 2D magnetic couplings, consistent with the spin-wave-corrected magnetic susceptibility, $J_{NN}=-2.44$ meV, $J_{NNN}=-1.22$ meV, $J_\perp=0$, $D=0.134$ meV, $D'=0.120$ meV, are shown in Fig. 2(c). The agreement between the model calculation and the experimental data is generally good. The decrease in intensity with increasing Q, due primarily to the magnetic form factor, is in agreement with experiment. The model calculation has the peak of the scattering map at slightly higher energy and smaller wave vector than the experimental results.

Note that the choice of model interaction parameters is constrained by the requirement of magnetic stability $-J_{NNN}\le-(J_{NN}+J_\perp)/2$. It is not possible to lower the calculated energy of the peak, into better agreement with experiment, by making J_{NNN} more negative without violating this stability requirement.

We have also considered 3D magnetic couplings, i.e., $J_\perp$ nonzero. Because of the smaller spin-wave renormalization, the fit to a 3D model consistent with the magnetic susceptibility is significantly worse. Consider the extreme case of $J_\perp=J_{NN}=1.5$ meV. Figure 3(c) shows that, for parameters just at the edge of magnetic stability, the dominant $(0\ \frac{1}{2}\ 0)$ ZB energy is 12.5 meV. The asymmetry of the density of states shifts the peak to slightly higher energy, 14 meV. It is expected that the spin-wave renormalization effects would be predominantly 3D even for $J_\perp$, a rather small fraction of J_{NN}. These results therefore provide indirect evidence of the 2D nature of the magnetic couplings.

This analysis is rather sensitive to the spin-wave renormalization of the susceptibility and magnon spectrum. If $\Delta S/S$ is assumed to be larger than the values discussed above, it reduces J_{NN} determined from the susceptibility, which in turn lowers the expected energy of the magnon ridge seen in the neutron scattering results. The $i(\alpha)$ correction is less relevant: For a given value of the susceptibility, $i(\alpha)$ acts to lower J, but this is canceled by the increase in $E(\mathbf{q})$.

Another limitation inherent in the present treatment is the neglect of dynamical spin-strain couplings. It is possible that the hybridization of magnons and phonons is significant, and that the coupled spin-strain excitations have a lower energy that those of the spin-only system, without violation of the magnetic stability. Some work has been done along these lines,[22] but there is not yet any direct discussion of the stability issue.

The general agreement between model and experimental results shows that the 10-meV feature in the neutron scattering spectra is indeed dominated by the $(0\ \frac{1}{2}\ 0)$ ZB. In conclusion, the neutron inelastic scattering measurements on α-O_2 powder provide a direct measurement of the combination of exchange constants,

$$8(J_{NNN}-J_{NN}-J_\perp)+D=10\pm1\text{ meV}\ ,$$

and provide less direct evidence that $J_\perp/J_{NN}$ is small. We discuss the interpretation of this result in the context of other measurements and theory in Sec. IV.

C. β phase, quasielastic

The structure of β-O_2 is rhombohedral, made up of triangular sheets of molecules with the average molecular axes perpendicular to the sheets.[5] This structure is obtained from the α phase by relaxing the in-plane distortion, so that each molecule is surrounded by six neighbors separated by 3.30 Å. Molecules on a given plane are in the centers of triangles of molecules in the adjacent planes, with an *ABCABC* stacking sequence.

It is well known that the lowest energy for classical AF spins on a 2D triangular lattice is the three-sublattice Yaffet-Kittel[29] structure shown in Fig. 4. Several authors have pointed out the possible relevance of this structure to β-O_2.[30,31] The fact that each molecule is equally close to its three neighbors on each adjacent plane implies that there is rigorously zero magnetic coupling between adjacent planes of the Yaffet-Kittel structure, justifying the 2D description of this magnetic structure for β-O_2. However, in the first neutron diffraction work on β-O_2, Collins showed that there was no long-range magnetic order.[32] Later, Stephens *et al.* noted that the diffuse scattering observed by Collins is in the position of the expected $\sqrt{3}$ magnetic peak of the three-sublattice structure, implying that there is short-range magnetic order.[31]

We have investigated the nature of this short-range order in the β phase was quasielastic neutron scattering. Polarized neutron scattering, discussed below, establishes that this diffuse peak is indeed magnetic in origin. Figure 4 compares quasielastic scattering intensity in two- and three-axis modes of neutron analysis. In both cases, the incident neutron energy was 13.5 meV, with 20′ collimation. The two-axis configuration integrates over neutron energy changes, so that it measures *instantaneous* correlations between spins. The resulting spectra show a diffuse peak at the $\sqrt{3}$ position of 1.28 Å^{-1}. We observe no change in the shape of this peak between 27 and 41 K, essentially the full range of stability of β-O_2. On the other hand, in the triple-axis configuration, the energy resolution is 0.4 meV HWHM, and no peak in the diffuse scattering is observed. This indicates that the 1.29-Å^{-1} peak results from dynamical correlations, with an energy scale greater than 0.4 meV. We shall return to a discussion of the energy scale of these fluctuations below.

In view of the lack of coupling between layers in the Yaffet-Kittel spin structure, it is appropriate to discuss the instantaneous spin correlations in a 2D model. If there were long-range correlations in the plane, the diffraction from a powder would assume the characteristic sawtooth waveform first discussed by Warren.[33] This line shape has a sharp edge below the peak, which provides a measure of the correlation length, and a broad trailing edge, due to the projection of Bragg rods onto the scattering plane. The sharp leading edge is not observed in β-O_2, implying that the correlations have relatively short range. We assume that the spin correlations decay exponentially with a distance $1/\kappa$, and calculate the diffraction profile by averaging over crystallite orientations. We take the energy-integrated structure factor for a single plane to be given by

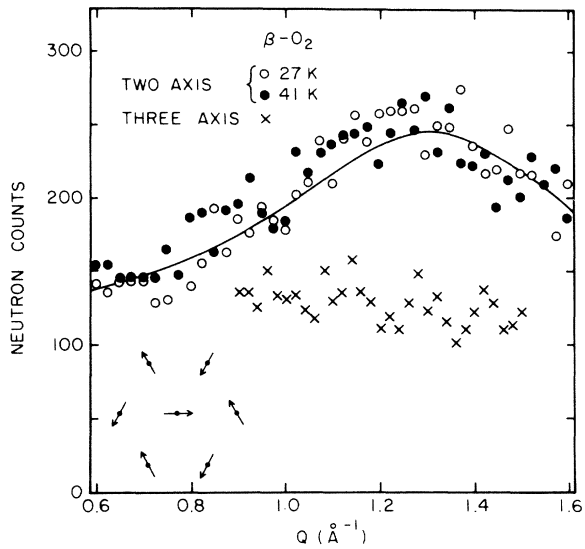

FIG. 4. Quasielastic scattering from β-O_2 in the region of the $\sqrt{3}$ magnetic wave vector. The smooth curve is a fit to a powder-averaged 2D Lorentzian, discussed in the text. The inset shows the three-sublattice magnetic structure, described for β-O_2.

$$S(\mathbf{Q})=\frac{\kappa^2}{\kappa^2+|\mathbf{Q}_2-\mathbf{q}_0|^2}\ , \tag{6}$$

where $\mathbf{Q}_2$ is the projection of $\mathbf{Q}$ onto the plane and $\mathbf{q}_0$ is the zone center of the $\sqrt{3}$ magnetic structure. The average over orientations is performed as described by Stephens *et al.*,[34] yielding an intensity proportional to

$$I(Q)=\int_0^{\pi/2} d\psi \cos\psi \int_0^{\pi/6} d\phi\, \kappa^2 F^2(Q,\pi/2-\psi)(\kappa^2+Q^2\cos^2\psi+q_0^2-2q_0Q\cos\psi\cos\phi)^{-1}\ , \tag{7}$$

where $F(Q,\beta)$ is the magnetic form factor of the O_2 molecule at scattering vector of magnitude Q at an angle β from the molecular axis.[27] The smooth curve in Fig. 4 shows the result of a fit with $1/\kappa=3.6\pm1.0$ Å and a constant background of 75 counts. The fitted value of κ depends strongly on the assumed background, causing the large uncertainty in κ. We note that the asymmetry of the Warren-model line shape is here masked by the rapidly decreasing molecular form factor.

D. β phase, inelastic

Having established the spatial extent of the magnetic correlations, we take up a discussion of their energy scale. Figure 5 shows the results of a polarized neutron scattering study, resolving the signal into nuclear and magnetic components. The neutron measurements were made in the same configuration as the α phase data of Fig. 2. The

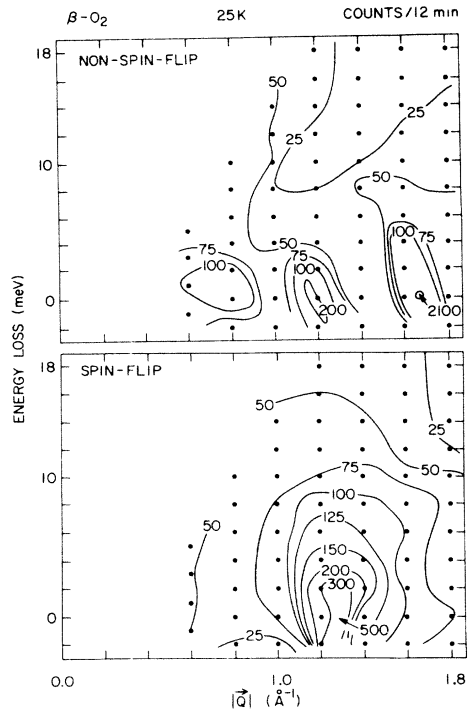

FIG. 5. Inelastic neutron spectra from powdered β-O_2.

non-spin-flip cross section shows the (003) Bragg peak at 1.67 Å^{-1} and the $(10\bar{1})$ Bragg peak visible at 1.18 Å^{-1}, due to second-order contamination in the beam. Because this second-order contamination is unpolarized, it makes a comparable contribution to the spin-flip measurement. The diffuse scattering centered around 1.3 Å^{-1} appears only in the spin-flip cross section, and has an energy scale of $\sim$6 meV. The energy resolution of these measurements is 2—2.5 meV HWHM, sufficiently poor to preclude a determination of whether the inelastic scattering peaks at zero or at finite-energy transfer.

Before discussing these results, we consider the magnetic scattering from a disordered magnet in two limiting cases. DeGennes has discussed the inelastic scattering from a paramagnet in the high-temperature limit.[35] For large momentum transfer, one expects a Gaussian distribution in energy, having a standard deviation

$$2[zS(S+1)]^{1/2}|J| \ . \tag{8}$$

The distribution becomes narrower and changes its shape as the scattered wave vector is reduced to values comparable to π/a, where a is the interspin separation. The energy-integrated dynamical structure factor, $\int S(Q,\omega)d\omega$, is independent of wave vector Q, so that the only dependence of the scattering cross section on Q is through the magnetic form factor. At the opposite limit is the case of critical scattering in a system with large spatial correlations. Such a system lacks long-range order, but correlated regions of size l produce a quasielastic peak of width l^{-1}, centered at the position of the Bragg peaks of the incipient ordered phase. The energy scale of this critical scattering decreases to zero as the correlations increase.

The case of β-O_2 appears to lie between these two extremes, with spatial correlations extending to one or two nearest neighbors. Interpolating between the experimental values for the α-phase exchange constants, one derives an in-plane exchange of -1.8 meV for β-O_2. When this result is substituted into Eq. (8), it predicts an energy scale of 7 meV HWHM for the paramagnetic scattering, in reasonable agreement with the results of Fig. 5.

IV. DISCUSSION

A. α phase

In Sec. III A we described the synthesis of inelastic neutron measurements with existing susceptibility data, which lead to the result that the intrasublattice exchange interaction, J_{NNN}, has magnitude which is half that of the total intersublattice exchange, $J_{\text{NN}}+J_{\perp}$. A direct interpretation of the susceptibility and neutron scattering results imply $J_{\text{NNN}}/J_{\text{NN}} > \frac{1}{2}$, but that would cause the magnetic structure to be unstable against the formation of a static spin wave along b^*.

A number of authors have argued that the magnetic interaction between adjacent planes is a small fraction of that within each plane of molecules.[15,16,21] None of the data presently available permits us to quantify the ratio $J_{\perp}/J_{\text{NN}}$; however, based on the apparent magnetic transition temperature, one can argue that the interactions are principally 2D.

It is useful to review the nature of the magnetic order in quasi-2D magnets. While it is well known that the 2D Heisenberg model does not have long-range order at any finite temperature, 3D magnets comprised of weakly coupled magnetic sheets aquire 3D magnetic order as a consequence of the growth of 2D magnetic correlations. This magnetic transition takes place well below the mean-field ordering temperature,

$$T_{\text{MF}} = 2S(S+1)z\,|J|/3 \ .$$

For example, consider the Heisenberg $S=1$ antiferromagnet, K_2NiF_4, for which the ratio of inter- to intraplanar exchanges is on the order of 10^{-6}.[3,9] This magnet orders at 36% of T_{MF}, compared with 72% for the analogous 3D system, $KNiF_3$. Other quasi-2D magnets surveyed by DeJongh and Miedema[9] with $S \geq 1$ have T_c/T_{MF} in the range 0.36—0.48.

In the case of α-O_2, the data of Fig. 1 shows that the magnetic system would disorder at a temperature of $\sim$30 K if the α-β transition did not intervene. DeFotis arrived at a comparable value for the hypothesized loss of magnetic order in α-O_2 by extrapolating to the point where the parallel and perpendicular susceptibilities become equal.[2] Taking the (2D spin-wave corrected) value of $J_{\text{NN}} = -2.4$ meV and considering only the nearest-neighbor interaction, α-O_2 has $T_{\text{MF}} = 100$ K. Including the correction to the total exchange from J_{NNN} lowers this by 25% to 75 K. The extrapolated ordering temperature of 30 K is 40% of this value. This agreement with other quasi-2D magnets is quite good. On the other hand, the ratio is well outside of the range of 3D Heisenberg magnets, 0.70 to 0.81.[9] It is therefore clear that the loss

of magnetic order in α-O_2 is inconsistent with $J_\perp/J_{NN}$ on the order of unity, although a quantitative estimate of this ratio is not possible. In any event, the proximity of the extrapolated critical temperature to the expected value for 2D couplings leads us to regard the spin-wave correction to the susceptibility and magnon energies as being correctly given by the 2D values of ΔS and $i(0)$.

We next discuss the single-spin anisotropy terms, D and D'. As shown in Table I, these govern the $\mathbf{q}=\mathbf{0}$ antiferromagnetic resonance (AFMR) energies. The measured values of the two $\mathbf{q}=\mathbf{0}$ energies, 0.8 and 3.4 meV, together with exchange constant $J_{NN}=-2.4$ meV, leads to the values $D+D'=0.25$ meV, $D-D'=0.014$ meV.

The single-molecule term in the spin Hamiltonian, Eq. (1), has energy eigenvalues 0, $-(D-D')$, and $-(D+D')$. This Hamiltonian describes a system with easy-plane anisotropy in the case that $D=D'$, so that the single-spin term has a twofold degenerate excited state with energy $2D$ above the ground state. In the present case, this excited state is split by anisotropy within the easy plane, $D'\neq D$. The fine-structure splitting in an isolated O_2 molecule is 0.5 meV,[18] twice the value of $D+D'$ that we infer from the AFMR energies.

The relatively weaker in-plane anisotropy may be compared with the magnetic dipole energy. For a two-sublattice antiferromagnet of classical point magnetic dipoles, the energy per spin is given by

$$E_{\text{dipole}}=\tfrac{1}{2}\mu^2\sum_i \pm\frac{1-3(\hat{\boldsymbol{\mu}}\cdot\hat{\mathbf{r}}_i)^2}{r_i^3}\ ,$$

where $\mu=2\mu_B$ is the magnetic moment of an oxygen molecule with a g factor of 2, the sum runs over all lattice sites $\mathbf{r}_i$, and the sign in each term is taken as $+$ for spins on the same, $-$ on the opposite magnetic sublattice. The factor $\frac{1}{2}$ avoids double counting the lattice sum. Considering only the 12 nearest neighbors, this magnetic energy per spin is -0.013 meV for spins pointing along $\pm\hat{\mathbf{x}}$, 0.016 meV along $\pm\hat{\mathbf{y}}$, and -0.003 meV along $\pm\hat{\mathbf{z}}$. Further neighbors make a significant contribution. We have calculated the energy by summing over all sites within a circle of radius r_c, and have checked for convergence as $r_c\to\infty$. There is no systematic effect of r_c on energy for $r_c>12$ Å; however, one must go out to 30 Å for fluctuations of the estimated energies to be less than 1%, as r_c is varied. The sums converge to -0.009, 0.014, and -0.005 meV for spins oriented in the x, y, and z directions, respectively. The observed spin direction along $\hat{\mathbf{x}}$ therefore minimizes the magnetic dipole energy. Meier *et al.* have calculated a dipole energy difference of 0.021 meV between the $\hat{\mathbf{x}}$ and $\hat{\mathbf{y}}$ orientations, in basic agreement.[17] This is close to the value determined from the spin-flop field.[17]

If we identify the difference in energy for classical spins pointing along $\hat{\mathbf{x}}$ and $\hat{\mathbf{y}}$ with $D-D'$, the dipole contribution to the anisotropy is $D-D'=0.023$ meV, nearly twice that inferred from the AFMR energies.

We therefore see that both the in-plane and out-of-plane anisotropy energies derived from the spin-wave spectrum of α-O_2 are approximately half the expected values. These differences could be due to intermolecular crystal-field effects, or to systematic error in the quantum corrections to the magnon spectrum. Because the anisotropies are a relatively small fraction of the intermolecular exchange, it is possible that magnetic coupling to nearby molecules affects the single-spin energies. It would be interesting to see if crystal-field energies can be derived from the present level of understanding of O_2 molecular wave functions and interactions.[21] On the other hand, quantum corrections to the magnon spectrum may need to be refined. In Lindgard's analysis, the anisotropies are multiplied by a finite spin correction term $1-1/2S$.[12,36] For the present case with $S=1$, it is possible that truncation of this series may make a significant change to the anisotropies derived from the magnon spectrum.

B. β phase

Experimentally, β-O_2 is a paramagnet, with some degree of short-range spin order in a three-sublattice structure. From the measured α-O_2 magnetic exchange parameters, we can estimate the nearest-neighbor exchange in β-O_2. Assuming a power-law dependence of exchange on intermolecular separation, $J(R)\propto R^{-n}$, the parameters for α-O_2, $J(3.20\ \text{Å})=-2.44$ meV and $J(3.43\ \text{Å})=-1.22$ meV, leads to an estimate of $n\cong 10$ and a β-O_2 exchange $J(3.30\ \text{Å})=-1.8$ meV.

Lee *et al.* have considered the classical planar antiferromagnet on a triangular lattice, and have found that the three-sublattice state is stable below a transition temperature $\cong -J$.[37] For β-O_2, that predicts an estimated transition temperature of 21 K. It therefore appears that the α-β transition preempts the formation of three-sublattice magnetic order.

The extent of the magnetic correlations well above this presumed transition point is a consequence of the 2D nature of the system. Other quasi-2D magnets such as K_2NiF_4 show strong magnetic fluctuations well above their critical temperatures.[3] Indeed, in the present case, frustration appears to be more important than thermal disorder in destroying the spin order, and so it is not surprising that the correlation length is independent of temperature, as shown in Fig. 4.

C. α-β transition

In the previous sections we have described the measurement of the magnetic interactions in α- and β-O_2. Numerous authors have suggested that the distortion of α-O_2 from the triangular structure of β-O_2 takes place in order to maximize the magnetic energy by readjusting the distances to neighbors on the same and opposite sublattices.[30,31,38,39] We now present a simple model for the α-β transition in the light of these observations.

Consider an initially triangular array of spins, subject to elastic and magnetic interactions between near neighbors. The total energy is given by

$$H=\sum_{\langle ij\rangle}\tfrac{1}{2}C(R_{ij}-R_0)^2-2\sum_{\langle ij\rangle}J(R_{ij})\mathbf{S}_i\cdot\mathbf{S}_j\ . \tag{9}$$

Here R_0 is the unstrained bond length, C is the stiffness, and $J(R_{ij})$ is a distance-dependent exchange, assumed negative, which grows weaker with increasing separation. In order to obtain an analytically solvable model, we linearize $J(R)$ as

$$J(R_{ij}) = -|J_0|[1-n(R_{ij}-R_0)/R_0] .$$

We minimize the energy by variation of the parameters for various assumed spin structures. Consider first the three-sublattice structure, for which $\mathbf{S}_i \cdot \mathbf{S}_j = -\frac{1}{2}$ for all neighbors. It is useful to introduce the ratio of magnetic to elastic energy scales

$$j = 2n^2 |J_0| / CR_0^2$$

and the strain

$$u_{ij} = (R_{ij}-R_0)/R_0 .$$

For the three-sublattice structure, it is intuitively clear that the strain is uniform, so that the reduced energy per particle,

$$e_3 = E/N|J_0| = 3n^2u^2/j - 3 + 3nu .$$

This is minimized for a uniform contraction $u = -j/2n$, giving $e_3 = -3-3j/4$. One can also consider a two-sublattice phase, having the structure of a single plane of α-O_2. In this case, the energy must be minimized with respect to two different strains, u_1 between opposite sublattices, and u_2 on the same sublattice. The reduced energy of this phase, e_2, takes the minimum value $-2-3j$ for strains $u_2 = -u_1 = j/n$.

If one now imagines varying j, there will be a first-order transition between two- and three-sublattice phases when the two energies are equal, which occurs at $j = \frac{4}{9}$. At this transition, the ratio of intra- to intersublattice exchanges,

$$J(R_0(1+u_2))/J(R_0(1+u_1)) ,$$

is $\frac{5}{13}$.

We establish the connection between this model and the phases of solid oxygen by assuming that the temperature affects j via the sublattice magnetization. β-O_2 lacks long-range magnetic order; consequently, it is not precisely the three-sublattice phase of this simple model. This difference will change the value of j at the transition. The predicted value of $\frac{5}{13}$ for the ratio of exchange parameters is significantly less than the observed $\frac{1}{2}$. With a related model, Etters *et al.* predicted that the ratio of exchanges should be 0.253.[38]

This model predicts that in the two-sublattice phase, the strain $u_2 = -u_1 = j/n$, which is therefore proportional to the square of the magnetization. Krupskii *et al.*[5] have published accurate measurements of the temperature dependence of the lattice parameters of α-O_2. Based on these data, we have computed the strain, defined as $(r_2-r_1)/(r_2+r_1)$, where r_1 and r_2 are the nearest and next-nearest (equivalently, inter- and intrasublattice) distances in the plane. According to the simple model presented here, the strain should be equal to j/n. It is plotted in Fig. 1. At the transition, the strain takes the value 0.0337. Taking the critical value of j to be $\frac{5}{13}$, this implies $n = 11.4$, a reasonable agreement with other measurements. On the other hand, it is clear that the strain is not proportional to the square of the magnetization as the temperature is reduced. This effect could be due to the neglect of fluctuations in the model, or to anharmonic elastic interactions. It would be interesting to see whether the more detailed model of Etters *et al.* can account for the connection between magnetization and strain.[38]

Monolayer and bilayer films of O_2 physiadsorbed on graphite basal planes have a transition at 11.5 K which is similar to the α-β transition in bulk solid O_2.[40] This vastly different ordering temperature in the literally 2D system appears to challenge the model put forth here that the phase-transition properties of solid O_2 can be quantitatively understood on the basis of a 2D model. However, a closer examination shows significant differences between the adsorbed film phases and their bulk analogues. The film ζ phase, stable above 11.5 K, is not a thin layer of β-O_2. Different experiments support different models of the ζ phase; high-resolution x-ray diffraction is consistent with a model of two mutually incommensurate triangular layers,[41] while low-energy electron diffraction results imply that the ζ-phase film is stable for one monolayer, and has a slightly strained triangular structure.[42] The magnetically ordered[40] ϵ phase has an in-plane strain which varies from 0.023 to 0.029 as the temperature is lowered below the ζ-ϵ transition.[40,41] This is significantly smaller than the distortion in α-O_2. Taken in conjunction with the power-law form for $J(R)$ discussed above, this range of strains predicts the $J_{NNN}/J_{NN} = 0.56$–0.64, which violates the magnetic stability requirement. It is therefore likely that the magnetic structure of adsorbed O_2 films are different from the bulk system, vitiating the comparison between bulk and adsorbed film transition temperatures.

In conclusion, we have found that the structure of the α phase of solid O_2 follows naturally from the competition of the van der Waals interaction between O_2 molecules, favoring a triangular in-plane structure, and the antiferromagnetic interaction, which is satisfied when each molecule is surrounded by immediate neighbors having oppositely directed spins. As a consequence of this mechanism, J_{NNN} is a substantial fraction of J_{NN}. We have presented the first quantitatively consistent picture of the magnetic behavior of α- and β-O_2.

ACKNOWLEDGMENTS

We are pleased to acknowledge important contributions to the collection of the data and the interpretation of the results from R. J. Birgeneau and G. Shirane. Peter Heller kindly furnished the sample of MnF_2 discussed in the Appendix. This research was supported by the Research Corporation and by National Science Foundation Low Temperature Physics Grant No. DMR-8208570; work at Brookhaven National Laboratory was supported by the Department of Energy under Contract No. DE-AC02-7680016.

APPENDIX: MAGNETOVIBRATIONAL COUPLING

Magnetovibrational (MV) coupling, in which a neutron couples magnetically to lattice motions, is a potential artifact in this work. In this appendix, we describe the effect in general, showing that it has the expected polarization behavior and intensity relative to nuclear phonon and magnon signals. We then discuss its possible magnitude

in the inelastic magnetic scattering measurements described in Sec. III B.

A two-sublattice AF has magnetic diffraction peaks at reciprocal-lattice vectors τ_M which have zero intensity for nuclear diffraction. The sign of the interaction between the neutron and the localized magnetic moments alternates between the two sublattices, producing constructive interference at reciprocal-lattice vectors where the nuclear amplitudes interfere destructively. The magnetically scattered neutrons can gain or lose energy to lattice motions, through the annihilation or creation of phonons. This produces phonon branches with the antiferromagnetic Bragg peaks at the zone centers, as illustrated in Fig. 6(a).

Because the neutron has coupled to the system magnetically, the selection rules for polarized neutrons are the same as for the corresponding Bragg peaks. Consequently, for neutron spin aligned along the scattering vector, MV scattered neutrons should appear in the spin-flip channel.[23]

As simple as these arguments may seem, we are unaware of any previous experimental demonstration of MV scattering in an antiferromagnet. Accordingly, we performed a brief study of the effect in MnF_2.

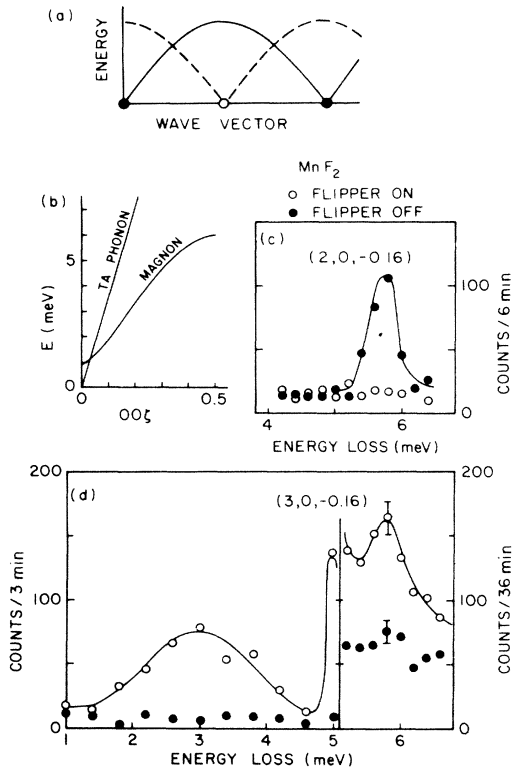

FIG. 6. (a) Bragg peaks and dispersion curves in an antiferromagnet. Solid dots and lines arise from nuclear scattering. Open circle is an antiferromagnetic Bragg peak, and dashed line is a MV phonon. (b) Dispersion curves of transverse-acoustic phonon and magnon in MnF_2. (c) Inelastic polarized neutron scan in a zone containing a nuclear Bragg peak, showing the phonon in the non-spin-flip channel. (d) Scan in an antiferromagnetic zone, showing magnon and MV phonon, both in the spin-flip channel.

The spectrometer configuration was essentially the same as described in the text of this paper, with Heusler alloy monochromator and analyzer, 40′ collimation, constant final neutron energy of 31 meV, and a flipping ratio of 23.

The dispersion curves of a transverse-acoustic phonon and magnon are sketched in Fig. 6(b). Figure 6(c) is an inelastic scan near the nuclear (200) zone center, showing the phonon with an energy of 5.8 meV. In the magnetic zone [Fig. 6(d)], we observe a magnon at 3 meV,[43] as well as the same 5.8-meV phonon. As expected, both inelastic peaks are spin-flip in the magnetic zone.

It is of interest to compare the intensities of MV and conventional nuclear phonon scattering. The nuclear cross section for an unpolarized neutron to create a phonon is[13]

$$\frac{d^2\sigma}{d\Omega\, dE'} = \frac{k_f}{k_i}\frac{(2\pi)^3}{2v_0\omega_j(\mathbf{q})}\left|\sum_d b_d e^{i\mathbf{Q}\cdot\mathbf{d}}\mathbf{Q}\cdot\boldsymbol{\sigma}_d^j(\mathbf{q})M_d^{-1/2}\right|^2 \times e^{-2W}[n(\hbar\omega)+1]\delta(\omega-\omega_j(\mathbf{q}))\delta(\mathbf{Q}-\mathbf{q}-\tau)\ . \tag{A1}$$

Here j is the branch index, d indexes the nuclei in one unit cell, M_d and b_d are the mass and scattering length of the dth nucleus, and $\hbar\omega_j(\mathbf{q})$ is the energy of the phonon. e^{-2W} and $n(\hbar\omega)$ are the Debye-Waller and Bose factors, respectively. The dimensionless polarization vectors, $\boldsymbol{\sigma}_d^j(\mathbf{q})$ give the relative amplitude and phase of the motion of the dth nucleus.

The corresponding MV cross section is obtained by replacing b_d by $\pm p$ for each magnetic site, where the magnetic scattering length

$$p=(\gamma e^2/2m_e c^2)g\langle J\rangle F(\mathbf{Q})\ .$$

Here $\gamma=1.91$ is the neutron magnetic moment in nuclear magnetons, and g, J, and $F(\mathbf{Q})$ are the g factor, angular momentum, and magnetic form factor. The cross section is multiplied by an overall factor $(1-\hat{\mathbf{Q}}_x^2)$, where $\hat{\mathbf{Q}}_x$ is the cosine of the angle between the scattering vector and the spin direction.

By studying an acoustic phonon at small $\mathbf{q}$, the displacement is identical at all sites, so we replace $\boldsymbol{\sigma}_d^j(\mathbf{q})M_d^{-1/2}$ by σ, which is in the (100) direction in the present case.

At the position of an antiferromagnetic Bragg peak, e.g., (300), the nuclear scattering completely vanishes. However, there is a nuclear scattering component for $\mathbf{q}\neq 0$. With neutron spin parallel to $\mathbf{Q}$, there is no magnetic-nuclear interference, and so one may consider the nuclear (non-spin-flip) and magnetic (spin-flip) interactions separately. Thermal fluctuations diminish the spin $\langle J\rangle$ 70% below its saturated value of $\frac{5}{2}$ at the experimental temperature of 50 K.[44] Together with the form factor from Ref. 45, this leads to a magnetic scattering length $p=0.30\times 10^{-12}$ cm. Based on Eq. (A1), we calculate that the ratio of spin-flip to non-spin-flip cross sections is 3.0 at (3,0,−0.16), and the ratio of spin-flip at (3,0,−0.16) to non-spin-flip at (2,0,−0.16) is 0.15. The

non-spin-flip peak at $(3,0,-0.16)$ is not visible with the experimental signal to noise of Fig. 6(d), but the ratio of peak intensities in magnetic to nuclear zones is 0.13 ± 0.05, in agreement with the expected ratio.

For a discussion of the relative significance of MV and magnon scattering in α-O_2, we need to derive the ratio of MV to magnon scattering cross sections. From Eqs. (5) and (A1), the ratio of MV to magnon cross sections at a given wave vector $\mathbf{Q}$ is

$$\frac{1-\hat{Q}_x^2}{1+\hat{Q}_x^2}\frac{2\hbar}{\omega_j(\mathbf{q})}\frac{\left|\sum_d \pm e^{i\mathbf{Q}\cdot\mathbf{d}}\mathbf{Q}\cdot\boldsymbol{\sigma}_d^j(\mathbf{q})M_d^{-1/2}\right|^2}{(u_\mathbf{q}\pm v_\mathbf{q})^2}. \tag{A2}$$

Here $\hbar\omega$ is the phonon energy; the magnon energy enters only through $u_\mathbf{q}$ and $v_\mathbf{q}$. In the case of experiments performed at constant k_f with a monitor after the monochromator, this gives the ratio of integrated intensities of the two inelastic peaks. Substituting the appropriate parameters for the two excitations shown in Fig. 6(d), the predicted ratio of MV phonon to magnon integrated intensities is 0.022, in agreement with the experimentally observed value 0.025 ± 0.010.

Having established that the MV scattering from an antiferromagnet has the expected intensity and polarization dependence, we turn to a discussion of the possible effect of MV scattering in the interpretation of our data on α-O_2. Specifically, we need to address the possibility that the 10-meV inelastic peak is due to MV rather than magnons. Without knowing the phonon polarization vectors, we can still argue that the strongest possible phonon scattering occurs when $\boldsymbol{\sigma}$ is parallel to $\mathbf{Q}$, and each term in the sum of Eq. (A2) contributes in phase. The numerator of the third factor of Eq. (A2) is then bounded by Q^2/M, where $M=16$ amu. The interpretation of Sec. III B is based on the assignment of the 10-meV feature as a zone boundary magnon, for which $(u\pm v)^2=2$ for each of the two (degenerate) branches. Equation (A2) then predicts that the *maximum possible* ratio of MV to magnon scattering at 1.6 Å^{-1} and 10 meV is 0.04. It is therefore clear that magnon scattering overwhelmingly dominates MV scattering at the wave vectors studied in α-O_2, and that the magnetic feature seen at 10-meV energy loss represents an inelastic process in the magnetic system, not the lattice.

There is one remaining detail regarding the applicability of Eq. (A2). Because α-O_2 is a molecular solid, there is a group of relatively soft librons, involving tilting motion of the molecules. The one phonon cross section is derived under the assumption that $Q^2\langle u^2\rangle$ is sufficiently small that its exponential may be approximated by the first two terms in the Taylor series. The largest published estimate for the zero-point rms librational angle is 19° along one direction.[38] The experimental temperature of 10 K is sufficiently below the libron gap of 60 K (Ref. 46) that the amplitude is unlikely to exceed significantly this zero point value. $Q^2\langle u^2\rangle$ is therefore at most 0.07, justifying the neglect of multiphonon terms.

[1] P. W. Stephens, R. J. Birgeneau, C. F. Majkrzak, and G. Shirane, Phys. Rev. B **28**, 452 (1983).

[2] G. C. DeFotis, Phys. Rev. B **23**, 4714 (1981).

[3] R. J. Birgeneau, H. J. Guggenheim, and G. Shirane, Phys. Rev. B **1**, 2211 (1970).

[4] C. N. Yang, Phys. Rev. **85**, 808 (1952).

[5] I. N. Krupskii, A. I. Prokhvatilov, Yu. A. Freiman, and A. I. Erenburg, Fiz. Nizk. Temp. **5**, 271 (1979) [Sov. J. Low Temp. Phys. **5**, 130 (1979)].

[6] C. S. Barrett, L. Meyer, and J. Wasserman, J. Chem. Phys. **47**, 592 (1967).

[7] In their neutron diffraction study, Meier and Helmholdt [Phys. Rev. B **29**, 1387 (1984)] observed a weak (010) diffraction peak and concluded that the spin is rotated from the crystal *b* axis. However, they ignored a number of stronger peaks which could not be indexed, and so it is not clear how much confidence to place in this result. A small deviation of the spin from the *b* axis will not affect the conclusions of this paper.

[8] F. Keffer, in *Handbuch der Physik*, edited by H. P. J. Wijn (Springer, New York, 1966), Vol. 23.

[9] L. J. deJongh and A. R. Miedema, Adv. Phys. **23**, 1 (1974), also published as *Experiments on Simple Magnetic Model Systems* (Taylor and Francis, London, 1974).

[10] M. E. Lines, J. Phys. Chem. Solids **31**, 101 (1970); J. H. P. Colpa, E. G. Sieverts, and R. H. van der Linde, Physica **51**, 573 (1971).

[11] R. J. Meier, C. J. Schnikel, and A. deVisser, J. Phys. C **15**, 1015 (1982). Note that unrationalized magnetic units are used in this paper.

[12] P. A. Lindgard, R. J. Birgeneau, J. Als-Nielsen, and H. J. Guggenheim, J. Phys. C **8**, 1059 (1975). Note that the sign of the J_0' term in the magnon dispersion relation is reversed in this paper.

[13] W. Marshall and S. W. Lovesey, *Theory of Thermal Neutron Scattering* (Oxford, London, 1971).

[14] E. J. Wachtel and R. G. Wheeler, Phys. Rev. Lett. **24**, 233 (1970); J. Appl. Phys. **42**, 1581 (1971).

[15] I. A. Burakhovich, I. N. Krupskii, A. I. Prokhvatilov, Yu. A. Freiman, and A. I. Erenburg, Pis'ma Zh. Eksp. Teor. Fiz. **25**, 37 (1977) [JETP Lett. **25**, 32 (1977)].

[16] V. A. Slyusarev, Yu. A. Freiman, and R. P. Yankelevich, Pis'ma Zh. Eksp. Teor. Fiz. **30**, 292 (1979) [JETP Lett. **30**, 270 (1979)]; Fiz. Nizk. Temp. **6**, 219 (1980) [Sov. J. Low Temp. Phys. **6**, 105 (1980)].

[17] R. J. Meier, J. H. P. Colpa, and H. Sigg, J. Phys. C **17**, 4501 (1984). The magnon dispersion relation in this paper is manifestly incorrect, as it does not reduce to the well-known ferromagnetic expression when J_{NNN} dominates, and J_{NNN} incorrectly appears in the $\mathbf{q}=\mathbf{0}$ antiferromagnetic resonance frequencies.

[18] M. Tinkham and M. W. P. Strandberg, Phys. Rev. **97**, 937 (1955).

[19] A. Landau, E. J. Allin, and H. L. Welsh, Spectrochim. Acta **18**, 1 (1962); Yu. B. Gaididei, V. M. Loktev, A. F. Prikhot'ko, and L. I. Shanskii, Fiz. Nizk. Temp. **1**, 1365 (1975) [Sov. J. Low Temp. Phys. **1**, 653 (1975)].

[20] R. Bhandari and L. M. Falicov, J. Phys. C **6**, 479 (1973).

[21] M. C. van Hemert, P. E. S. Wormer, and A. van der Avoird, Phys. Rev. Lett. **51**, 1167 (1983); P. E. S. Wormer and A. van

der Avoird, J. Chem. Phys. **81**, 1929 (1984).

[22]A. P. J. Jansen and A. van der Avoird, Phys. Rev. B **31**, 7500 (1985).

[23]R. M. Moon, T. Riste, and W. C. Koehler, Phys. Rev. **181**, 920 (1969).

[24]V. A. Slyusarev, Yu. A. Freiman, and R. P. Yankelevich, Fiz. Nizk. Temp. **7**, 536 (1981) [Sov. J. Low Temp. Phys. **7**, 265 (1981)].

[25]Marshall and Lovesey (Ref. 13) treat the case of uniaxial anisotropy, $D'=0$. We have made the logical extension by including D' in the same term as which it appears in the magnon energies. Note that their expression for the magnon cross section contains an incorrect factor of N, the number of (magnetic) unit cells in the crystal. We have defined u_q and v_q without the factor of N.

[26]The usual density of neutron states factor k_f/k_i does not appear in an experiment performed at fixed k_f; see N. J. Chesser and J. D. Axe, Acta Crystallog. Sec. A **29**, 160 (1973).

[27]P. W. Stephens, Phys. Rev. B **31**, 4491 (1985). This paper discusses errors in several previous determinations of the O_2 magnetic form factor.

[28]M. J. Cooper and R. Nathans, Acta Crystallog. **23**, 357 (1967).

[29]Y. Yaffet and C. Kittel, Phys. Rev. **87**, 290 (1952).

[30]V. M. Loktev, Fiz. Nizk. Temp. **5**, 295 (1979) [Sov. J. Low Temp. Phys. **5**, 142 (1979)].

[31]P. W. Stephens, P. A. Heiney, R. J. Birgeneau, P. M. Horn, J. Stoltenberg, and O. E. Vilches, Phys. Rev. Lett. **45**, 1959 (1980); P. A. Heiney, P. W. Stephens, S. G. J. Mochrie, J. Akimitsu, R. J. Birgeneau, and P. M. Horn, Surf. Sci. **125**, 539 (1983).

[32]M. F. Collins, Proc. Phys. Soc. London **89**, 415 (1966).

[33]B. E. Warren, Phys. Rev. **59**, 693 (1941).

[34]P. W. Stephens, P. A. Heiney, R. J. Birgeneau, P. M. Horn, D. E. Moncton, and G. S. Brown, Phys. Rev. B **29**, 3512 (1984).

[35]P. G. DeGennes, J. Phys. Chem. Solids **4**, 223 (1958).

[36]P. A. Lindgard and O. Danielsen, J. Phys. C **7**, 1523 (1974); P. A. Lindgard and A. Kowalska, *ibid.* **9**, 2081 (1976).

[37]D. H. Lee, J. D. Joannopoulos, J. W. Negele, and D. P. Landau, Phys. Rev. Lett. **52**, 433 (1984).

[38]R. D. Etters, A. A. Helmy, and K. Kobashi, Phys. Rev. B **28**, 2166 (1983).

[39]Yu. B. Gaididei and V. M. Loktev, Fiz. Nisk. Temp. **7**, 1305 (1981) [Sov. J. Low Temp. Phys. **7**, 634 (1981)]; B. Kuchta, Phys. Lett. **103A**, 202 (1984).

[40]J. P. McTague and M. Nielsen, Phys. Rev. Lett. **37**, 596 (1976); M. Nielsen and J. P. McTague, Phys. Rev. B **19**, 3096 (1979).

[41]S. G. J. Mochrie, M. Sutton, J. Akimitsu, R. J. Birgeneau, P. M. Horn, P. Dimon, and D. E. Moncton, Surf. Sci. **138**, 599 (1984).

[42]M. F. Toney and S. C. Fain, Jr., Phys. Rev. B **30**, 1115 (1984); H. You and S. G. Fain, Jr. (to be published).

[43]G. G. Low, A. Okazaki, R. W. H. Stevenson, and K. C. Turberfield, J. Appl. Phys. **35**, 998 (1964).

[44]P. Heller, Phys. Rev. **146**, 403 (1966).

[45]C. G. Shull and E. O. Wollan, in *Solid State Physics,* edited by F. Seitz, D. Turnbull, and H. Ehrenreich (Academic, New York, 1956), Vol. 2.

[46]J. E. Cahill and G. E. Leroi, J. Chem. Phys. **51**, 97 (1969).